Electronic Supplementary Material (ESI) for Journal of Materials Chemistry
This journal is © The Royal Society of Chemistry 2011

Highly Exposed and Activity Modulated Sandwich Type Pt Thin Layer Catalyst with Enhanced Utilization

Beena K Balan and Sreekumar Kurungot *

Physical and Materials Chemistry Division, National Chemical Laboratory, Pune, India 411008.

E-Mail: k.sreekumar@ncl.res.in; Fax: +91 20 25902636 Tel: +91 20 25902566

Supporting Information:

Results

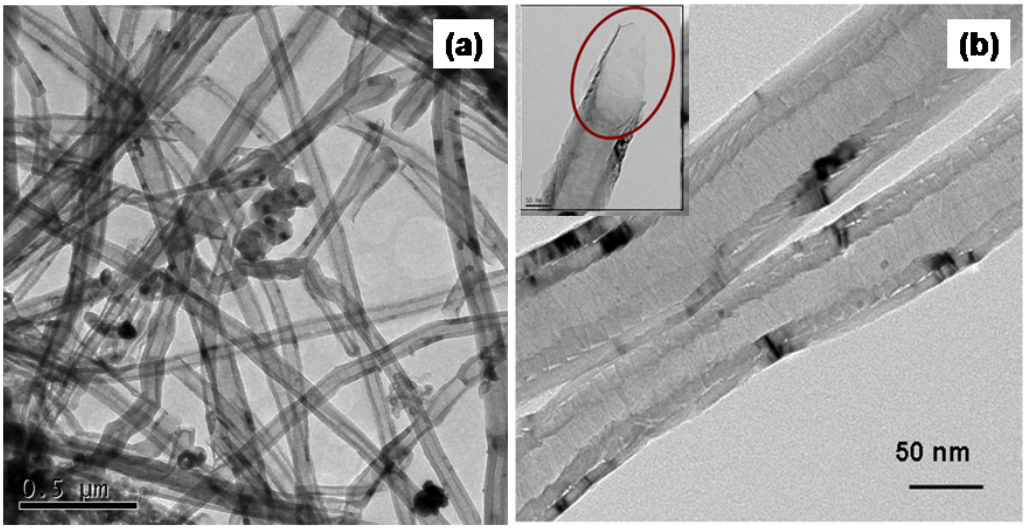

Figure S1: HRTEM images of high aspect ratio carbon nanofibers, (a) low magnification image showing the length of nanofibers in few micrometers and diameter ca. 100 nm. (b) high magnification image showing the inactive outer wall and active terminal grapheme edges in the inner cavity, image in the inset shows the open tips of the carbon nanofibers

Figure S1 shows the HRTEM images of pristine carbon nanofiber support at various magnifications. Fig S1 (a) , the low magnification image shows that the length of CNFs is in few micrometers and diameter about 100 nm. The peculiar morphology characteristics of CNFs, which enables the complete access of inner cavity is clear from

This journal is © The Royal Society of Chemistry 2011

the high magnification image given in (b). Here the active terminal edges in the inner cavity and the deposition of the thick carbon layer on the outer wall is clearly depicted. Further, the open tips of these CNFs are also clear from the image given in the inset o Figure S1 (b).

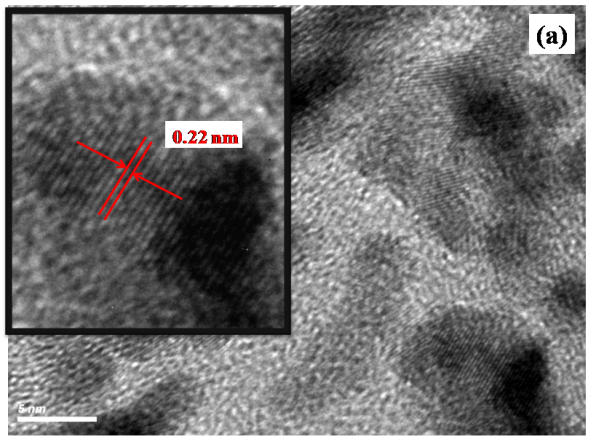

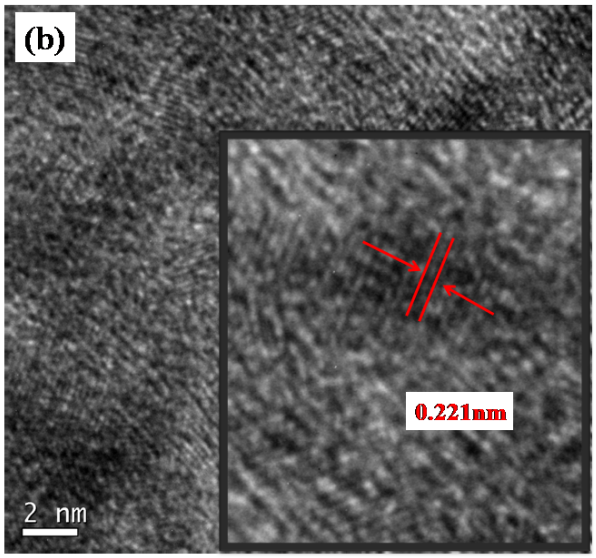

This journal is © The Royal Society of Chemistry 2011

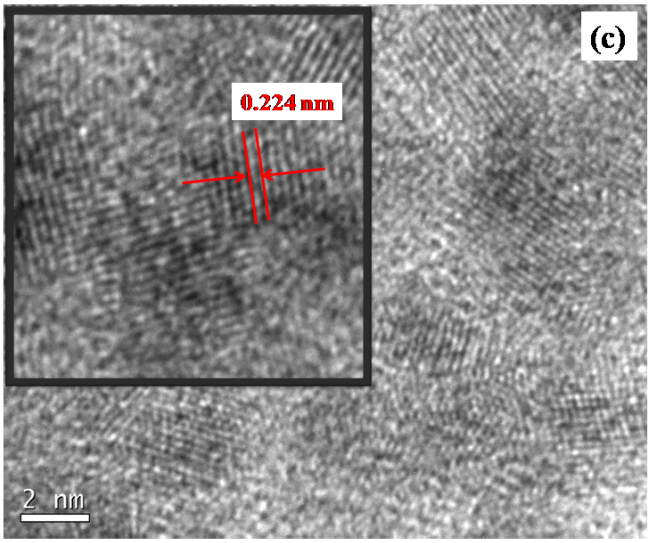

Figure S2: HRTEM images obtained for (a) F-Pt, (b) F-$Pt_1Ru_{0.5}$ and (c) F-Pt_1Ru_2

HRTEM images of F-Pt, F-$Pt_1Ru_{0.5}$ and F-Pt_1Ru_2 with their clearly marked interplanar spacing in the inset of the respective figures are shown in Figure S2 (a, b and c) respectively. For all the catalysts, the *d*-value obtained is ca. 0.22 nm which matches with the (111) plane of fcc Pt. The interplanar spacing corresponding to RuO_2 cannot be measured due to its amorphous nature. In F-$Pt_1Ru_{0.5}$ and F-Pt_1Ru_2, the regions with lower contrast correspond to the exposed RuO_2. Fascinatingly, in F-Pt_1Ru_2, the lattice fringes corresponding to Pt are more resolved as compared to that in F-$Pt_1Ru_{0.5}$. This indicates the selective exposure of Pt towards the surface with increase in the Ru content in the bimetallic combinations.

This journal is © The Royal Society of Chemistry 2011

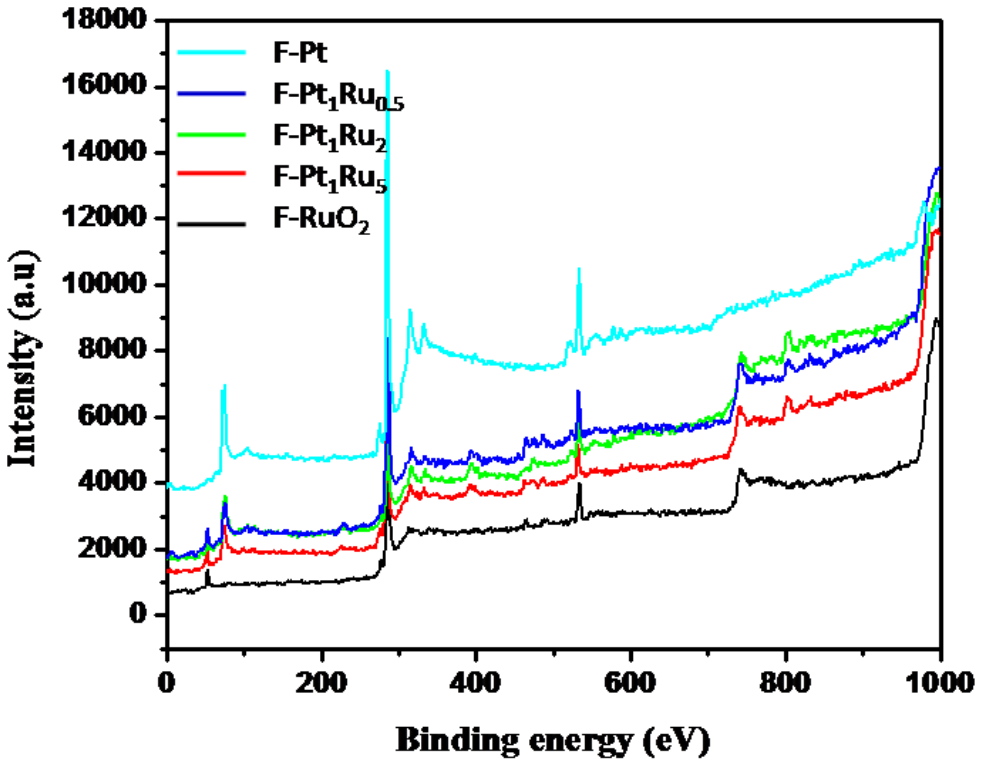

Figure S3: Full survey X-ray photoelectron spectra obtained for F-Pt (cyan), F-$Pt_1Ru_{0.5}$ (blue), F-Pt_1Ru_2 (green), F-Pt_1Ru_5 (red) and F-RuO_2 (black).

Table S1 compares the binding energy of C1s, Ru $3d_{5/2}$, Pt $4f_{7/2}$ and O1s levels after deconvolution of the XPS data shown in Figure S3. In all the catalysts, except F-Pt, the overlapped C 1s and Ru 3d core level regions after deconvolution gives five peaks, one corresponding to the graphitic carbon, two corresponding to the carbon attached to the oxygen containing functional groups and the remaining two corresponding to the Ru 3d core levels. The C 1s level of F-Pt gives three peaks after deconvolution corresponding to the graphitic carbon and carbon attached to functional groups. Ru, in all the catalysts is present exclusively in the form of RuO_2 and no metallic Ru is detected. Pt in F-Pt shows the presence of Pt(0) only whereas in all the bimetallic combinations Pt(0) and PtO are detected with a shift in binding energy. Oxygen is present in all the catalysts and on deconvolution it gives two peaks, one corresponding to the adsorbed oxygen and second

This journal is © The Royal Society of Chemistry 2011

corresponding to RuO_2. The absence of Pt in F-RuO_2, RuO_2 in F-Pt and chlorine in all catalysts is also clear from the XPS analysis.

Table S1: Deconvoluted X-Ray Photoelectron Spectra shows electron binding energies of C1s, Ru 3d and 3p, Pt 4f and O1s core levels for F-Pt F-$Pt_1Ru_{0.5}$, F-Pt_1Ru_2, F-Pt_1Ru_5 and F-RuO_2.

Sample	Carbon 1s	Ruthenium		Platinum 4f	Oxygen 1s
		3d	3p		
F-Pt	284.5 286.1 288.2	-		71.1 74.4	
F-$Pt_1Ru_{0.5}$	284.5 286 289.1	281.6 284	462.9 486.3 472.5	71.3 74.6 72.4 76.8	530.6 532.7
F-Pt_1Ru_2	284.5 285.9 289.3	281.6 285	463.2 485.7 472.5	71.4 74.8 72.6 76.7	530.3 532.3
F-Pt_1Ru_5	284.4 286 288	281.2 284.1	462.9 485.5 472.5	71.2 74.5 72.6 76.2	530.4 532.4
F-RuO_2	284.5 286 288.6	281.4 283.5	462.8 485.4	-	531.2 533.2

This journal is © The Royal Society of Chemistry 2011

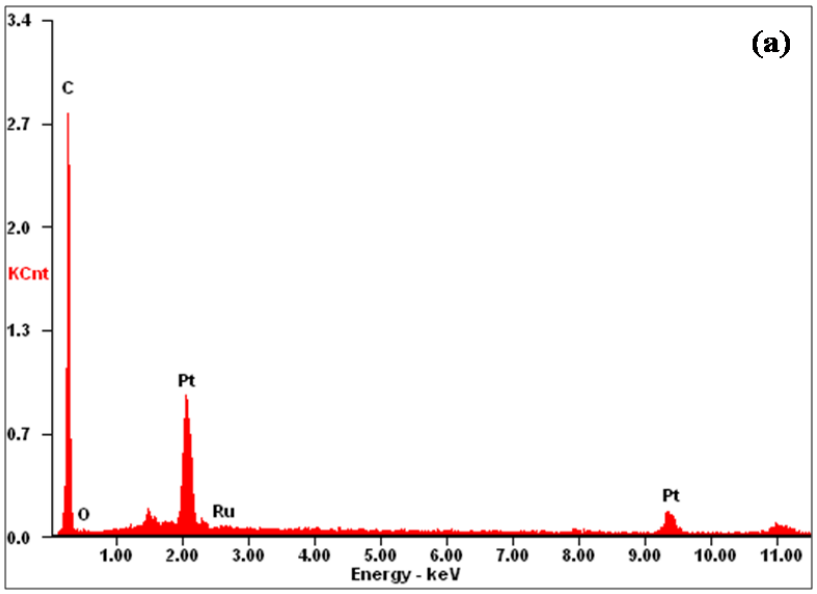

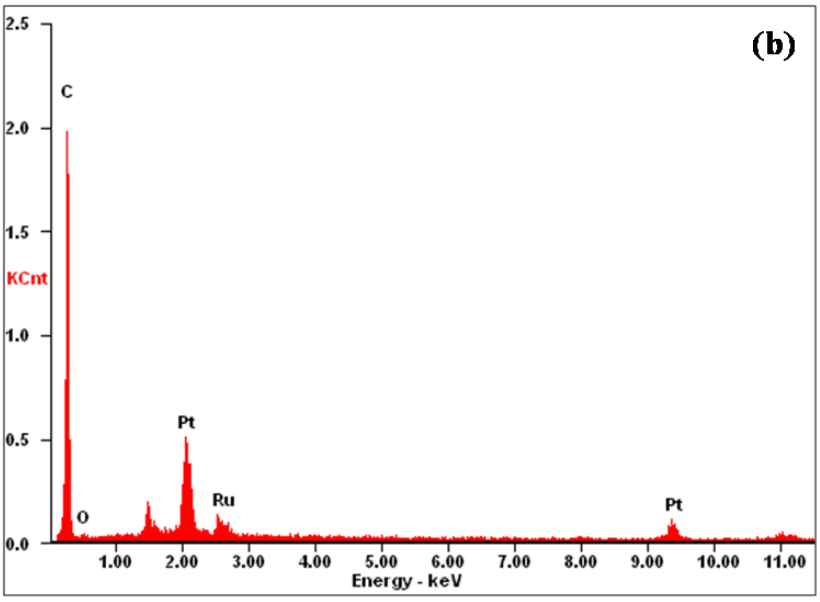

This journal is © The Royal Society of Chemistry 2011

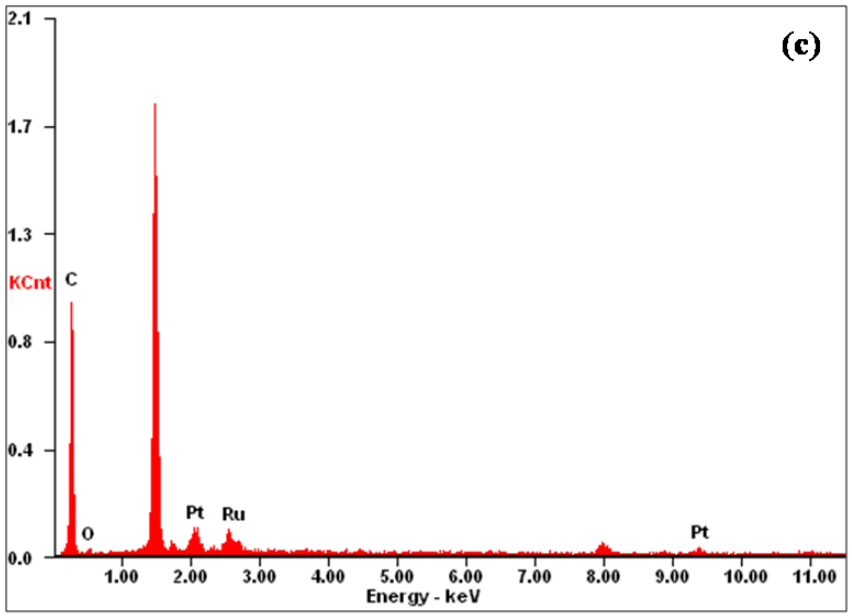

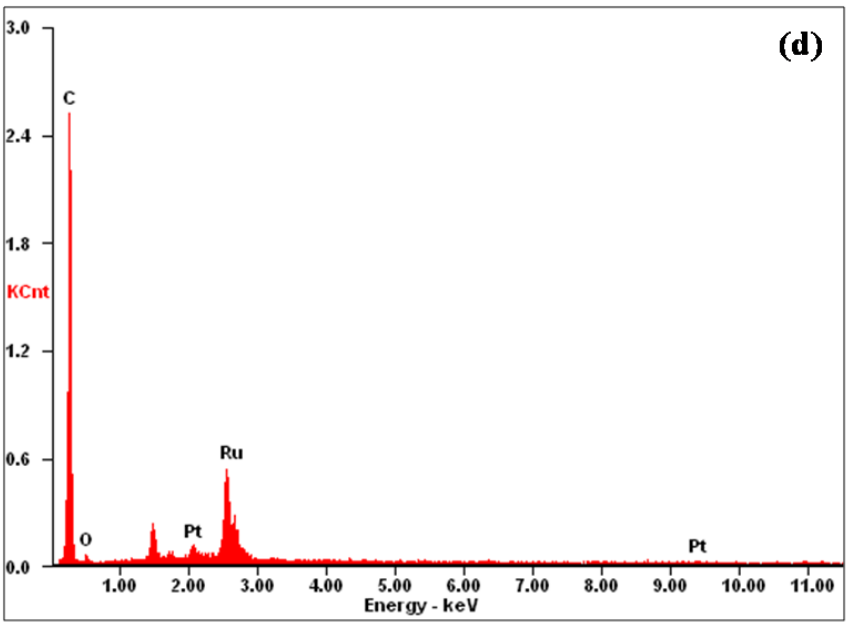

Figure S4: EDX spectrum of (a) F-Pt, (b) F-$Pt_1Ru_{0.5,}$ (c) F-Pt_1Ru_2 and (d) F-Pt_1Ru_5

As XPS is a surface sensitive technique, total loading on the carbon nanofiber support cannot be precisely determined using this tool. Therefore, energy dispersive X-ray (EDX) analysis of the samples with various Pt:Ru ratios is carried out and accordingly Figure S4 (a)-(d) show the EDX spectrum of F-Pt, F-$Pt_1Ru_{0.5,}$ F-Pt_1Ru_2 and

This journal is © The Royal Society of Chemistry 2011

F-Pt_1Ru_5. Table S2 summarises the EDX quantification report of these samples. In all the samples, carbon content remains almost same *ie.* 79-80 %. In F-Pt no traces of Ru is detected and the Pt content is 20 %. Almost negligible amount of oxygen (0.6%) is also detected in this sample. For F-$Pt_1Ru_{0.5}$, where the initial Pt:Ru ratio is 15:5, the EDX quantification gave the Pt:Ru ratio as 14.25:4.72. For the catalyst with the initial Pt:Ru weight ratio 10:10 (F-$Pt_1Ru_{0.5}$), the calculated ratio from EDX is 9.87:8.33. Finally, for F-Pt_1Ru_5, the EDX quantification gives the Pt:Ru ratio as 3.56:12.91. This is slightly less as compared to the initial Pt:Ru ratio of 5:15. The loading obtained for this catalyst from the TGA analysis is also slightly less than the initial loading and actually it displayed the lowest loading from the TGA analysis among all the catalysts. More fascinatingly, if we compare the oxygen contents in various bimetallic combinations, there is a progressive increase in the oxygen content with increase in the Ru content. This trend is also in complete agreement with the XPS results.

Table S2: EDX Quantification of F-Pt, F-$Pt_1Ru_{0.5}$, F-Pt_1Ru_2 and F-Pt_1Ru_5.

Sample	Carbon		Ruthenium		Platinum		Oxygen	
	Wt %	At %	Wt %	At %	Wt %	At %	Wt %	At %
F-Pt	79.02	97.85	00.00	00.00	20.33	01.55	00.65	00.60
F-$Pt_1Ru_{0.5}$	79.84	97.33	04.72	00.61	14.25	0.97	01.19	01.09
F-Pt_1Ru_2	79.09	95.71	08.33	1.23	09.87	00.70	02.71	02.36
F-Pt_1Ru_5	79.64	94.36	12.91	01.81	03.56	00.26	03.89	03.56

This journal is © The Royal Society of Chemistry 2011

The total loading on the carbon nanofiber support is further confirmed using TGA also. Figure S4 shows the TGA profile of pristine CNF, F-Pt, F-$Pt_1Ru_{0.5}$, F-Pt_1Ru_2 and F-Pt_1Ru_5 in air from room temperature to 1000 °C. The catalysts show initially a small weight loss corresponding to residual water followed by a continuous weight loss of carbon up to 700 °C. From the residue content, the loading amount (both Pt and RuO_2) is calculated to be 19.8, 19.5, 19.2 and 18.6 wt % respectively for F-Pt, F-$Pt_1Ru_{0.5}$, F-Pt_1Ru_2 and F-Pt_1Ru_5. It can also be noted from the TGA profile that, in case of pristine carbon nanofiber, no detectable amount of metal is present. Further, Ru is present in the form of RuO_2 only because if Ru is present in the metallic form, in presence of air TGA profile will show a weight gain corresponding to the formation of RuO_2. This feature gives an interesting evidence for the conclusion that Ru exists exclusively as RuO_2 in the catalyst.

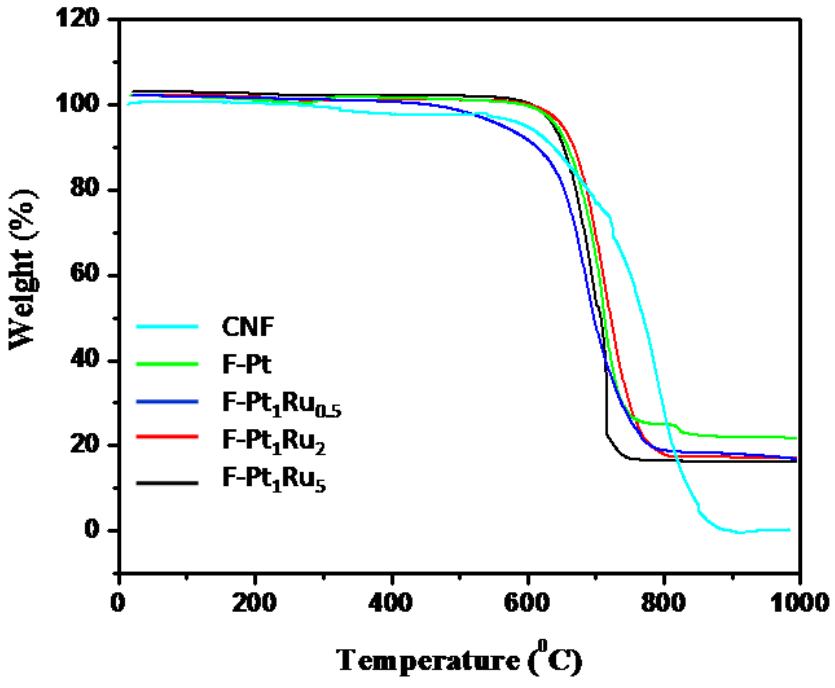

Figure S5: TGA profile obtained for pristine CNF, F-Pt, F-$Pt_1Ru_{0.5}$, F-Pt_1Ru_2 and F-Pt_1Ru_5 in air from room temperature to 1000 °C

This journal is © The Royal Society of Chemistry 2011

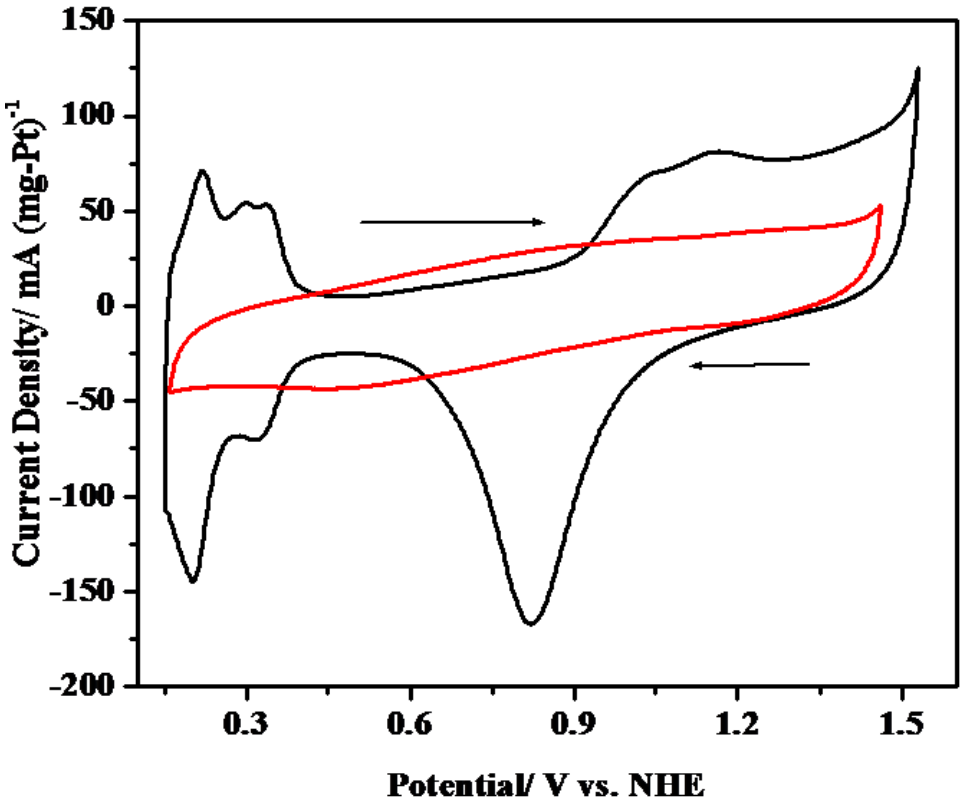

Figure S6: Comparison of cyclic voltammograms of F-Pt_1Ru_5 (black) and C-Pt_1Ru_5 (red) in 0.5 M H_2SO_4 at the scan rate of 50 mV/s.

The cyclic voltammograms of F-Pt_1Ru_5 and C-Pt_1Ru_5 recorded in 0.5 M H_2SO_4 clearly confirm the role of oxygen containing functional groups in enhancing the utilization of Pt (Figure S4). F-Pt_1Ru_5 shows CV features similar to that of a polycrystalline Pt electrode with the characteristic H_2 adsorption-desorption and oxide formation-oxygen reduction peaks. On the other hand, the CV of C-Pt_1Ru_5 shows typical capacitive behaviour exactly similar to that reported for hydrous RuO_2. This transition from the characteristic oxygen reduction behaviour of Pt to the characteristic capacitive features of RuO_2 clearly indicates that Pt is selectively exposed in F-Pt_1Ru_5 due to the preferential adsorption of Ru ions by virtue of the surface functional groups created during the pre-treatment process whereas in the case of C-Pt_1Ru_5 most of the Pt is merged in the RuO_2 layer

This journal is © The Royal Society of Chemistry 2011

completing suppressing its activity. Of course F-RuO_2 also shows features similar to that of C-Pt_1Ru_5 as shown in Figure S5, further confirming the role of oxygen containing functional groups in the design of the new catalyst for improving the Pt utilization.

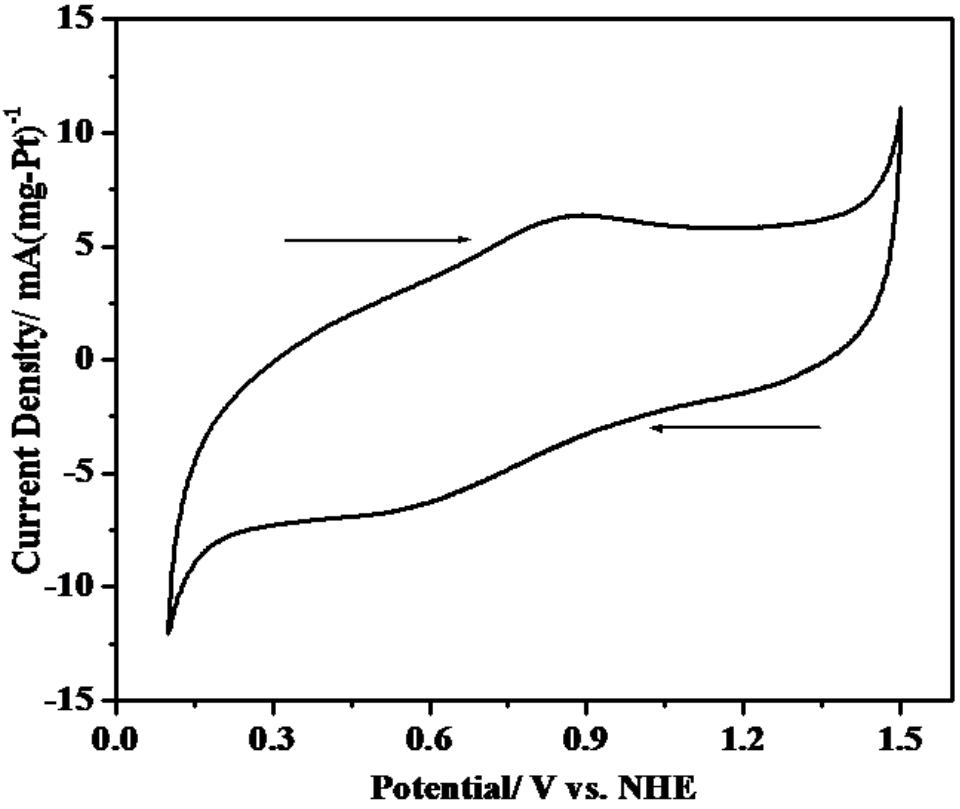

Figure S7: Cyclic voltammogram of F-RuO_2 in 0.5 M H_2SO_4 at the scan rate 50 mV/s.

The liner sweep voltammograms (LSV) obtained for F-Pt, F-$Pt_1Ru_{0.5}$, F-Pt_1Ru_2 and F-Pt_1Ru_5 for ORR in 0.5 M H_2SO_4 at a scan rate of 5mV/s are given in Figure S8 (a-d) respectively. The LSV is recorded at various rotation rates; 400, 900, 1200, 1600 and 2500 rpm. The limiting current is increased progressively with the rotating speed which is a characteristic feature of ORR. Normally, when the rotation speed increases, there will be an increase in the mass transfer rate of dissolved oxygen from bulk solution to the electrode surface and accordingly there will be an increase in the ORR activity with increase in the rotation rate.

This journal is © The Royal Society of Chemistry 2011

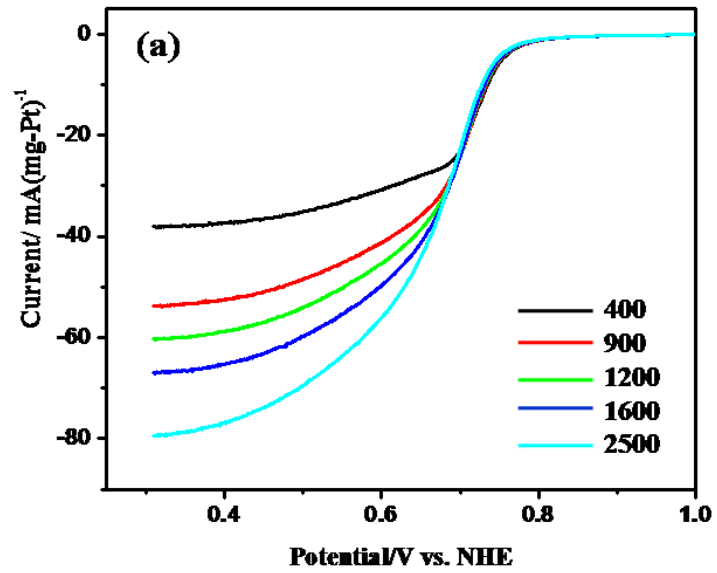

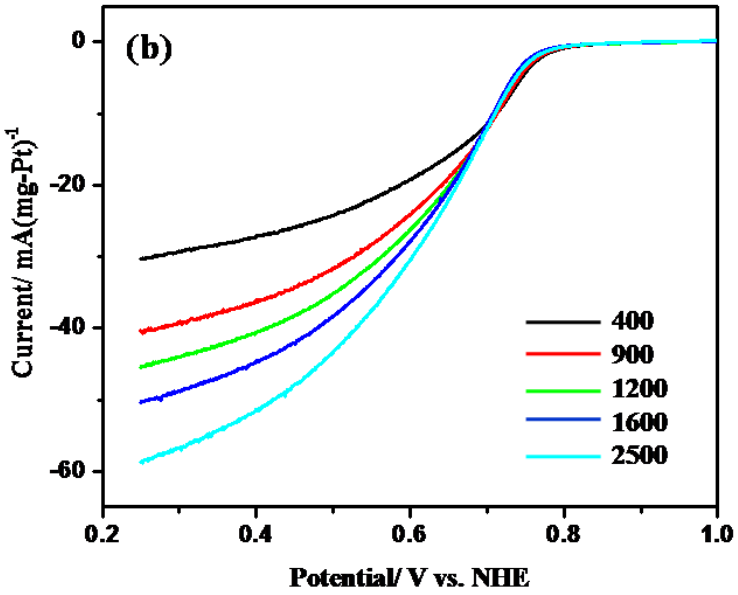

This journal is © The Royal Society of Chemistry 2011

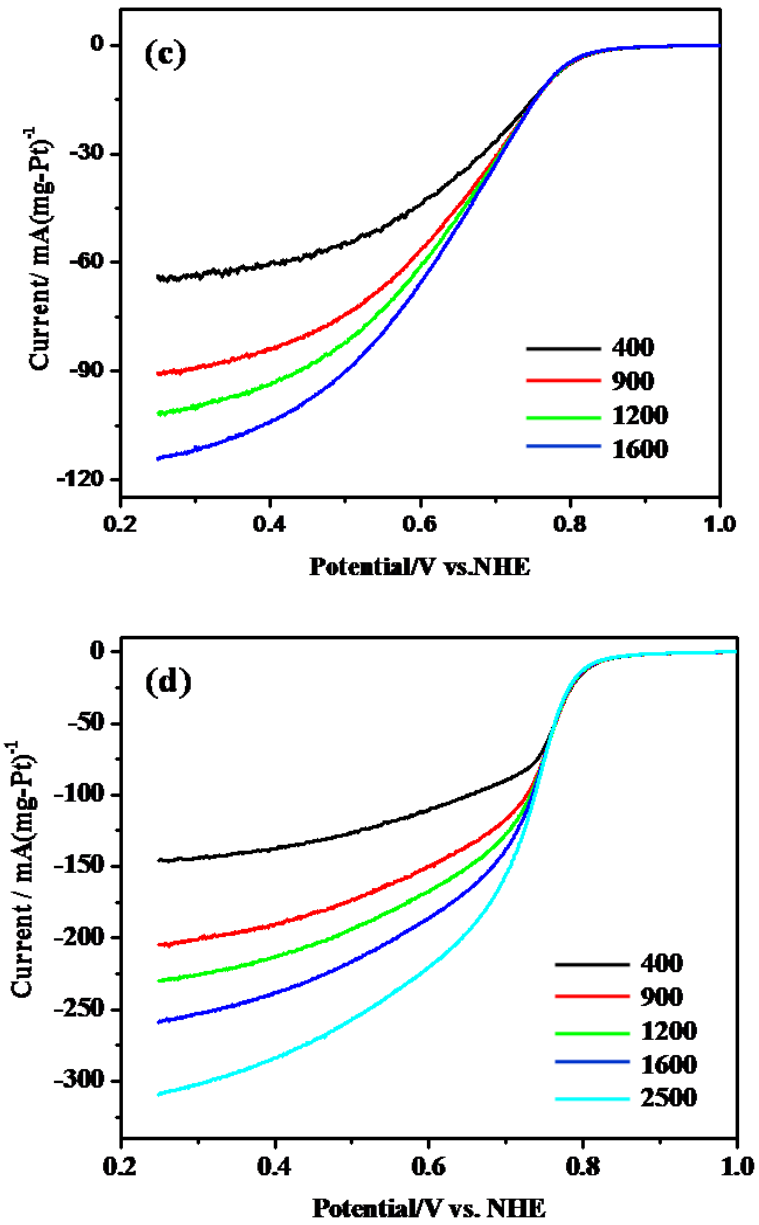

Figure S8: Linear sweep voltammograms obtained for (a) F-Pt, (b) F-$Pt_1Ru_{0.5,}$ (c) F-Pt_1Ru_2 and (d) F-Pt_1Ru_5 for ORR in 0.5 M H_2SO_4 with various rotating speeds at a scan rate of 5 mV/s.

Koutecky –Levich plots (K-L plots) *i.e.* a plot of the inverse current densities of ORR (j^{-1}) as a function of the inverse of the square root of rotating rate ($\omega^{-1/2}$) at various potentials are also presented. The overall current density (j) obtained will be the sum of

This journal is © The Royal Society of Chemistry 2011

the kinetic current density (j_k), diffusion-limited current density (j_d), and the film diffusion-limited current density of Nafion® (j_f). Since the amount of Nafion® is too low as compared to the total amount of the catalyst (for 10 mg of 20% catalyst we used 20 µl of 0.1 wt % Nafion®), j_f can be neglected. Thus, the overall measuring current density of ORR can be written as

$$\frac{1}{j} = \frac{1}{j_k} + \frac{1}{j_d} = \frac{1}{j_k} + \frac{1}{0.62nFAD_0^{2/3}C_0^{*}v^{-1/6}\omega^{1/2}}$$

where, 'n' is the electron transfer number, 'F' is the Faraday constant, 'D' is the diffusivity of O_2 in the electrolyte, 'C_O' is the O_2 concentration in the solution , 'v' is the kinematic viscosity and 'ω' is the rotating rate of RDE.

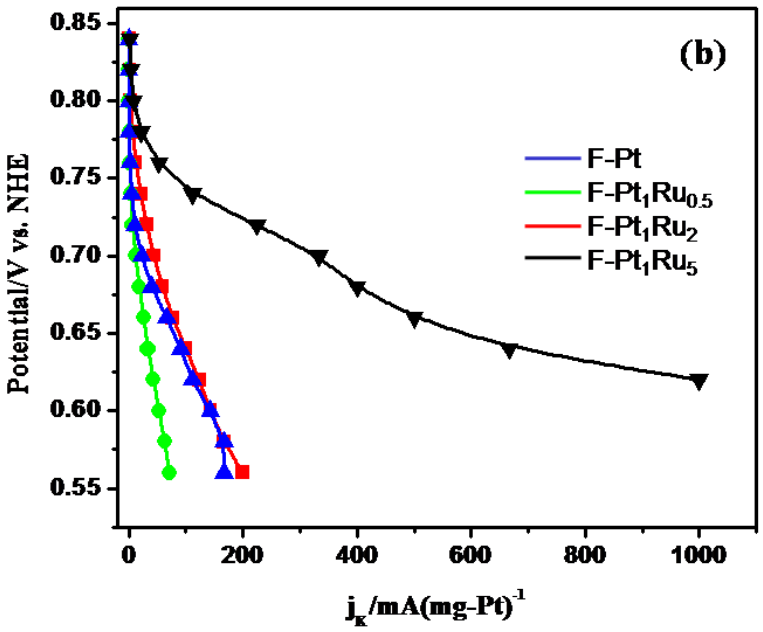

Figure S9: A plot of the limiting current values obtained from the Koutecky-Levich plots against the corresponding potential values.